Antiferroelectric Liquid-Crystal Gels

M. Carmen Artal, M. Blanca Ros,* and José Luis Serrano

Departamento de Química Orgánica, Facultad de Ciencias−ICMA, Universidad de Zaragoza−CSIC, 50009 Zaragoza, Spain

M. Rosario de la Fuente and Miguel Angel Pérez-Jubindo

Departamento de Física Aplicada II, Facultad de Ciencias, Universidad del País Vasco, 48080 Bilbao, Spain

Received December 20, 2000. Revised Manuscript Received March 7, 2001

The synthesis and characterization of several mesogenic antiferroelectric gels—obtained by in situ photopolymerization of mixtures of a nonchiral diacrylate and a nonreactive compound with an antiferroelectric SmC^*_A phase—is described. Along with kinetic aspects from their photopolymerization processes, information has been obtained concerning the dielectric permittivity, spontaneous polarization, optical response to an applied electric field, and the influence that the photopolymerization conditions and the structural characteristics of the network have on these properties. We have found that the polymer network not only stabilizes the antiferroelectric orientation but also alters the electro-optic properties of the liquid crystal.

Introduction

Owing to their fast switching and small driving voltages, ferroelectric (FLC) and antiferroelectric (AFLC) liquid crystals are suitable for several electro-optic applications. The polarization vector **P** tends to align parallel to the applied electric field, and because of the coupling between **P** and the preferential orientation of the molecules, this situation leads to the possibility of controlling the direction of the optical axis by the application of an electric field. For ferroelectric materials (SmC* phase) bistable switching behavior can be achieved. In the two stable states the optical axis is tilted with respect to the layer normal by an angle θ in opposite directions. For materials with an antiferroelectric phase (SmC^*_A), which is characterized by a anticlinic smectic structure, tristable switching is observed between the alternating state and two states of ferroelectric synclinic structure.[1]

The application of such materials in display technology suffers from the drawback of the high sensitivity of their uniform alignment to mechanical shock. One approach to overcome this problem is the stabilization of the molecular orientation by an anisotropic polymer network, giving rise to heterogeneous systems referred to as gels.[2] This type of gel is a fluid consisting of a solid tridimensional cross-linked network and a low molecular weight liquid crystal. The gel behaves thermally as a nonreactive liquid crystal. The network plays a role similar to the cell walls and has a significant influence on the nonattached molecules. To obtain good alignment, it is therefore necessary to obtain a well-aligned network. For this purpose, in situ photopolymerization is a very versatile technique.[3,4] A mixture of the reactive monomers plus the liquid crystal, a thermal inhibitor, and a photoinitiator that has mesogenic properties is introduced into a cell (prepared in a standard way, for example, to promote planar alignment). The material is held in the desired mesophase and is then illuminated with a suitable light source. The photochemical reaction takes place isothermally to give an oriented gel.

In this paper we present results on several mesogenic antiferroelectric gels obtained by in situ photopolymerization of mixtures of a nonreactive compound, which shows an antiferroelectric SmC^*_A phase, and a nonchiral diacrylate. From this study information was obtained concerning the dielectric permittivity, spontaneous polarization, optical response to an applied electric field, and the influence that the photopolymerization conditions and the structural characteristics of the network have on these properties. We found that the polymer network not only stabilizes the orientation but also alters the electro-optic properties of the liquid crystal.

To prepare the gels, the antiferroelectric compound (*R*)-1″-methylheptyl 4-(4′-*n*-decyloxybiphenyloxy)benzoate, hereafter called **f**, and the aromatic cross-linkers **a**, **b**, and the highly flexible diacrylate **c** were prepared (see Figure 1).

The main part of this research was focused on the characterization of gels based on 2 mol % of the cross-

* To whom correspondence should be addressed. E-mail: bros@posta.unizar.es.

(1) *Ferroelectric and Antiferroelectric Liquid Crystals*; Lagerwall, S. T., Ed.; Wiley-VCH: Weinheim, 1999.

(2) (a) Hikmet, R. A. M. *Mol. Cryst. Liq. Cryst.* **1991**, *198*, 357. (b) Hikmet, R. A. M. *Adv. Mater.* **1992**, *4*, 679. (c) Kelly, S. M. *Liq. Cryst.* **1998**, *24*, 71. (d) Dierking, I. *Adv. Mater.* **2000**, *12*, 167.

(3) Broer, D. J.; Boven, J.; Mol, G. N.; Challa, G. *Makromol. Chem.* **1989**, *190*, 2255.

(4) Broer, D. J. In *Radiation Curing in Polymer Science and Technology*; Fouassier, J. P., Rabek, J. F., Eds.; Elsevier Science Publishers Ltd.: London, 1993; Polymerisation Mechanisms, Vol. III, Chapter 12.

10.1021/cm001254m CCC: $20.00
Published on Web 05/30/2001

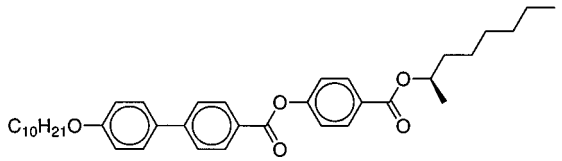

Compound **f**

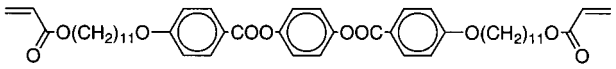

Crosslinker **a**

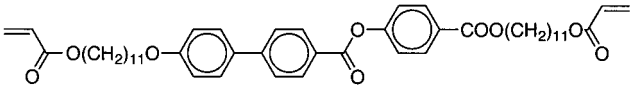

Crosslinker **b**

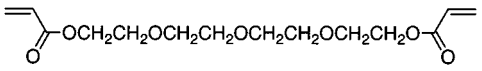

Crosslinker **c**

Figure 1. Chemical structure of the compounds used in the preparation of the antiferroelectric gels.

linker **b**, hereafter called **g/f-b2** (**g**, gel; **f**, antiferroelectric nonreactive component; **b2**, diacrylate that gives rise to the anisotropic network at 2 mol %). However, additional materials were prepared to analyze the influence of other aspects such as the chemical structure and percentage of compound within the network, and so results were obtained on analogous gels, namely, **g/f-a2**, **g/f-c2**, **g/f-a10**, and **g/f-b10**. It was found that good mixtures with diacrylate **c** could only be obtained when **c** was present in a low percentage.

Scheme 2

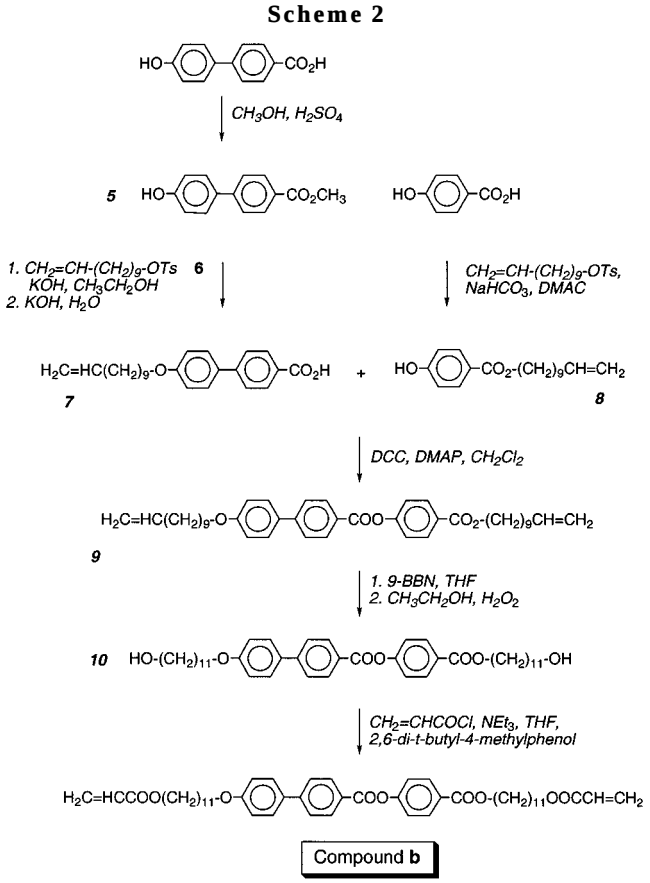

Compound **b**

Results and Discussion

Monomers and Photopolymerizable Samples. The nonreactive compound **f** and the diacrylates **a** and **b** were synthesized according to the synthetic routes shown in Schemes 1, 2, and 3, while compound **c** was commercially available.

Scheme 1

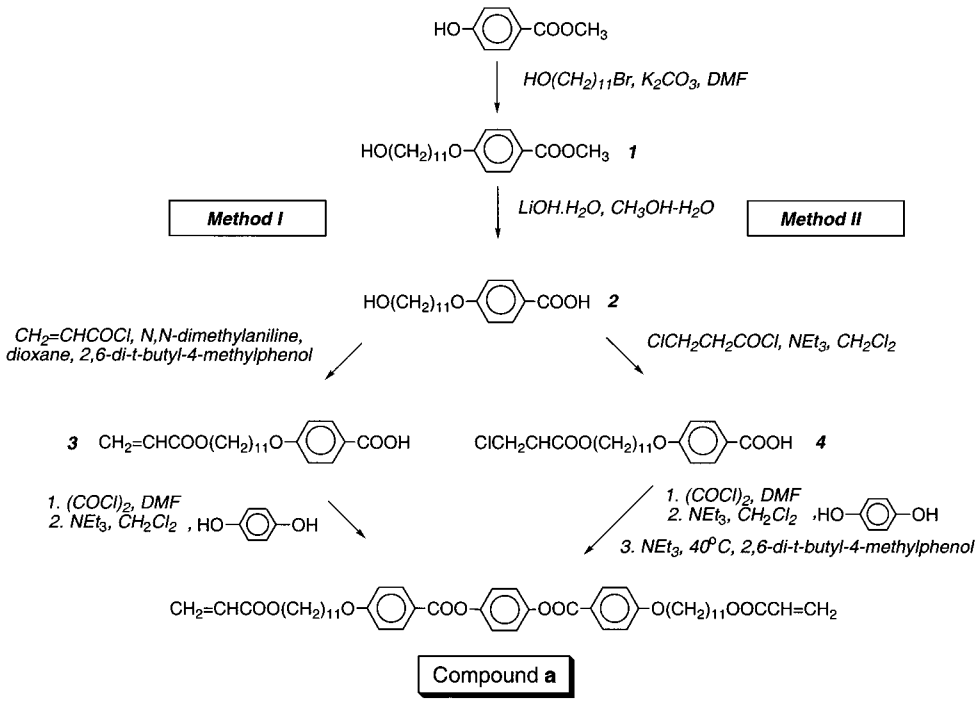

Compound **a**

Scheme 3

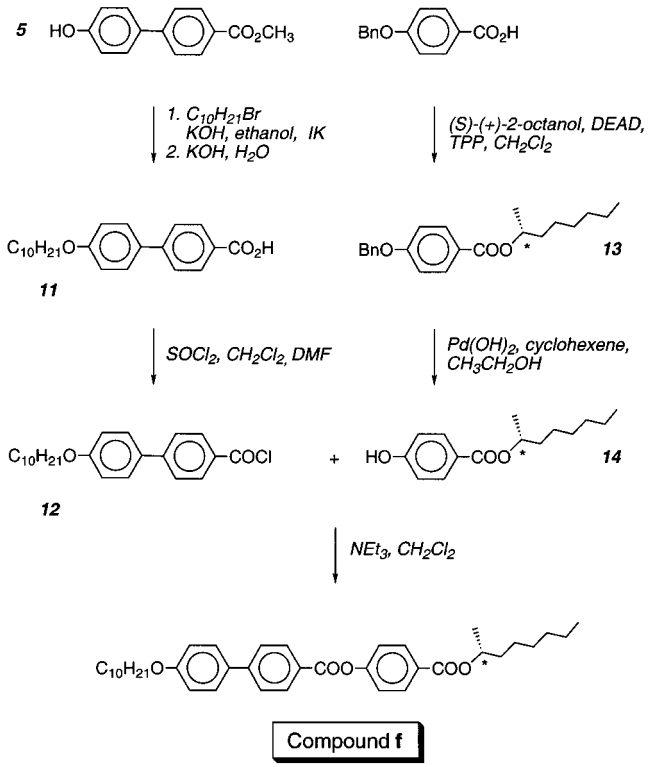

Two different approaches were used in the synthesis of compound **a**. Following method I,[3] acryloyl derivative **3** was obtained by the reaction of compound **2** with acryloyl chloride. Esterification of **3** with hydroquinone, via the acyl chloride, afforded compound **a**. In method II, 3-chloropropionyl chloride was reacted with compound **2** to give compound **4**, in which the chloropropionyl group acted as a precursor of the acryloyl group. Esterification of **4** with hydroquinone, followed by dehydrohalogenation using triethylamine in dichloromethane, led to compound **a**. Both methods provide similar yields, but method II is an interesting and new alternative to prevent lateral reactions of the acrylate group. It it useful when its incorporation should be made in the last synthetic step.

The acryloyl functionality was introduced into compound **b** by using a terminal double bond in the precursor. This system was converted into the primary alcohol in very high yields (95−99%) by the hydroboration−oxidation procedure described by Brown et al.[5] using 9-BBN as a hydroborating agent and with the modification reported by Sahlén et al.[6] to avoid the use of NaOH. Reaction of diol **10** with acryloyl chloride yielded compound **b**.

Compound **f** was synthesized by following methods similar to those reported in the literature for related compounds.

The mesomorphic properties and transition temperatures of the monomers were determined by polarizing optical microscopy (OM), differential scanning calorimetry (DSC), X-ray diffraction, and dielectric measurements. The results are collected in Table 1.

Table 1. Liquid-Crystal Properties of Pure Compounds[a]

compound	phase transition (°C, [kJ mol^{-1}])[b,c]
a	K 73.4 [66.29] SmE 84.9 [5.54] SmC 115.8 [1.16] N 136.7 [2.11] I
b	K 78.4 [63.50] SmC_{alt} 96.6[d] SmC 107.8 [0.13] SmA 117.3 [6.12] I
f[e]	I 134.8 [4.67] SmA 120.8 [0.39] SmC*$_\alpha$ 120.3 SmC* 112.9 [0.05] ferri-SmC*$_A$ 37.9 [0.74] SmI* 4.7 [9.20] K

[a] Compound **c** is liquid at room temperature. [b] K, crystalline phase; SmE, smectic E phase; SmC, smectic C phase; N, nematic phase; SmC_{alt}, alternating smectic C phase; SmA, smectic A phase; SmC*, chiral smectic C phase; SmI*, chiral smectic I phase; SmC*$_\alpha$ and SmC*$_\gamma$, chiral smectic C subphases; SmC*$_A$, antiferroelectric SmC phase; I, liquid phase. [c] Data determined by DSC: from second scans at a scanning rate of 10 °C/min. [d] Optical microscopic data. [e] Data from cooling scans.

The range of the SmC*$_\alpha$ phase of compound **f** is very narrow and lies between 120.8 and 120.3 °C. Its existence was confirmed by the presence of antiferroelectric behavior of the polarization current in switching experiments (two peaks regardless of the field frequency). As we shall show later, the transition from the SmC* to the SmC*$_A$ phase takes place via one or two ferrielectric phases, although the temperature ranges of these phases strongly depend on the sample thickness.

The phase sequence of the cross-linker **a** agrees with that previously reported for the same compound by Broer et al.,[7] with the exception of the SmE phase that was detected but not identified at that time.

Cross-linker **b** was synthesized for the first time during these studies and its physical characterization was reported elsewhere.[8] Interestingly, compound **b** shows a SmC_{alt} phase, the nonchiral, nonhelical version of the SmC*$_A$ phase.

The combination of data from OM, DSC, and dielectric studies allowed us to establish the phase transition sequence of the photopolymerizable binary mixtures used as precursors for the gels. The addition of the reactive monomers changed the phase transitions of the system to a small extent. From the experimental point of view, compound **f** and the polymerizable mixtures all exhibit very similar textures, thermograms, and dielectric spectra. From data corresponding to the blends only small changes in the transition temperatures were detected. As a representative example, the following sequence was determined for the mixture **f-b2**: I 131.1 °C SmA 118.0 °C SmC*$_\alpha$−SmC* 109.3 °C ferri-SmC*$_A$ 38.7 °C SmI* 0.4 °C K.

In Situ Photopolymerization Study of Photopolymerizable Samples. Neither compound **f** nor the diacrylates absorb above 360 nm and, consequently, the polymerization can be induced by a photoinitiator absorbing at 365 nm, the wavelength of emission of the lamp adapted to our photo-DSC experimental setup. For this reason, the DSC study of the photopolymerization of the mixtures was carried using samples containing 0.5% (w/w) of Irgacure 369, which absorbs at the appropriate wavelength (365 nm); 200 ppm of the

(5) (a) Brown, H. C.; Knights, E. F.; Scoten, C. G. *J. Am. Chem. Soc.* **1974**, *96*, 7765. (b) Brown, H. C.; Liotta, R.; Scoten, C. G. *J. Am. Chem. Soc.* **1976**, *98*, 5297.

(6) Sahlén, F.; Trollsås, M.; Hult, A.; Gedde, U. W. *Chem. Mater.* **1996**, *8*, 382.

(7) Broer, D. J.; Hikmet, R. A. M.; Challa, G. *Makromol. Chem.* **1989**, *190*, 3201.

(8) de la Fuente, M. R.; Martín, E.; Pérez Jubindo, M. A.; Artal, C.; Ros, B.; Serrano, J. L. *Liq. Cryst.* **2001**, *28*, 151.

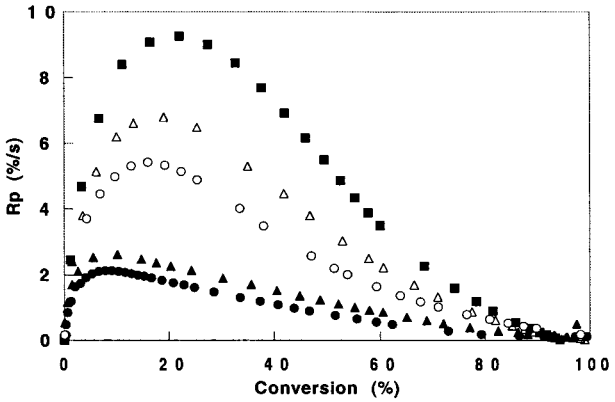

Figure 2. Polymerization rate vs conversion for different photopolymerizable samples at 80 °C in the SmC*$_A$ phase. [●] **f-a2**; [▲] **f-b2**; [■] **f-c2** ; [○] **f-a10**; [△] **f-b10**.

thermal inhibitor 2,6-di-*tert*-butyl-4-methylphenol was also added to avoid thermal polymerization. The samples were completely miscible in the range of concentrations investigated and their liquid-crystalline properties were not noticeably modified.

A study of the photopolymerization of the mixtures was carried out by DSC. The conversion versus irradiation time and polymerization rate versus conversion relationships were evaluated from the photopolymerization exotherms of the DSC curves. As an example, Figure 2 displays the dependence of the polymerization rate (R_p) on the conversion for different photopolymerizable samples at 80 °C in the SmC*$_A$ phase. As can be seen, the polymerization rate increases as the percentage of cross-linker increases because a higher degree of cross-linking hinders the mobility of macroradicals, thus increasing autoacceleration of the polymerization.[9] Additionally, a noticeably higher polymerization rate is observed for compound **c**, which is about 4 times faster than the photopolymerization of the two aromatic cross-linkers, both of which display similar curves. This phenomenon could be attributed to the short molecular length of compound **c**, which would allow higher mobility, as well as to a different type of segregation of the monomer between or in the smectic layers,[10] favoring the propagation step for a similar conversion degree. Nevertheless, these results differ from those reported in the literature for FLC gels,[10b] where the polymerization results are comparable for the various diacrylates used. On the other hand, the shift of fastest rate of polymerization toward the later conversion for high percentage of cross-linkers can be attributed to the concentration decrease of the reactive groups in the first steps of the polymerization. This makes further reactions more difficult in the 2% materials with the low-mobility cross-linkers.

Figure 3a,b shows, respectively, the dependence of the polymerization rate on the conversion of **f-b2** and **f-c2**, which were both photopolymerized in the SmA phase

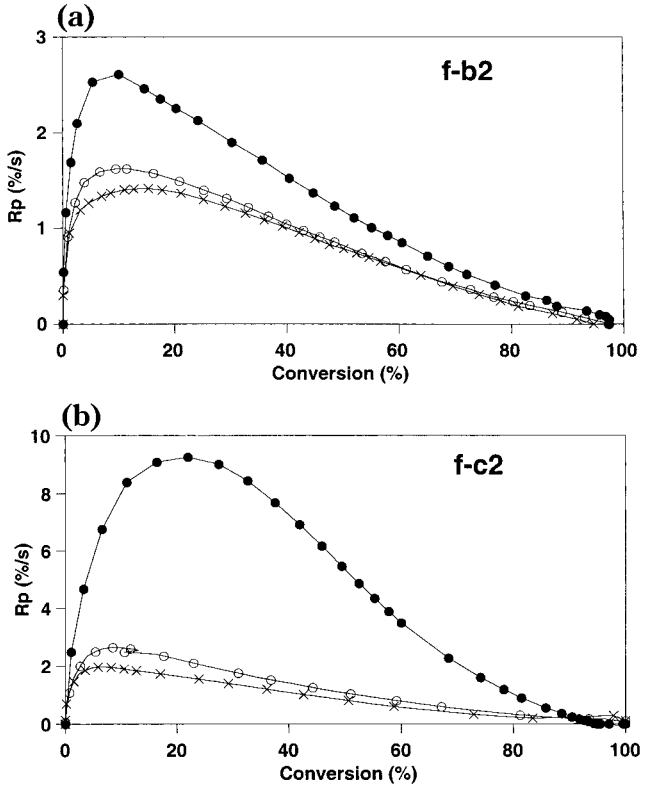

Figure 3. (a) Polymerization rate vs conversion for the samples **f-b2**, photopolymerized in the SmA phase (124 °C) [×], SmC* phase (112 °C) [○], and SmC*$_A$ phase (80 °C) [●]. (b) Polymerization rate vs conversion for the samples **f-c2**, photopolymerized in the SmA phase (124 °C) [×], SmC* phase (112 °C) [○], and SmC*$_A$ phase (80 °C) [●].

(124 °C), SmC* phase (112 °C), and SmC$_A$* phase (80 °C). The final conversion determined by DSC was higher than 95% regardless of the nature of the mesophase. A faster polymerization was observed with the antiferroelectric order (i.e., at the lowest temperature) for both cross-linking agents, while similar curves were observed for the polymerizations in the SmA and the SmC* phases. In general, these results agree with most reported data, which show that the higher the molecular order, the faster the polymerization process.[9−11] However, this trend changes with higher percentages of cross-linker (see Figure 4a,b) and in this region clear conclusions cannot be drawn. However, we believe that in this case the results cannot be attributed to the chemical structure of the diacrylate[9d] but rather to diffusional problems due to the high viscosity of the material and/or glass transitions during the photopolymerization process. On the other hand, compound **c** again gives rise to faster processes than the aromatic compounds **a** and **b**.

Dielectric and Optical Measurements. Apart from the aforementioned gels prepared in the SmC$_A$* phase, we aimed to study the possibilities of preparing antiferroelectric gels by modifying the experimental conditions of the photopolymerization. With this aim in mind, we prepared and characterized two new, different **g/f-b2** gels. One of these gels was obtained by photopolymerization at 80 °C (in the SmC$_A$* phase) under an electric field strong enough to give an unwound SmC*

(9) (a) Hikmet, R. A. M. *Liq. Cryst.* **1991**, *9*, 405. (b) Guymon, C. A.; Hoggan, E. N.; Walba, D. M.; Clark, N. A.; Bowman, C. N. *Liq. Cryst.* **1995**, *6*, 719. (c) Guymon, C. A.; Bowman, C. N. *Macromolecules* **1997**, *30*, 1594. (d) Guymon, C. A.; Shao, R.; Hölter, D.; Frey, H.; Clark, N. A.; Bowman, C. N. *Liq. Cryst.* **1998**, *24*, 263.

(10) (a) Guymon, C. A.; Hoggan, E. N.; Clark, N. A.; Rieker, T. P.; Walba, D. M.; Bowman, C. N. *Science* **1997**, *275*, 57. (b) Guymon, C. A.; Dongan, L. A.; Martens, P. J.; Clark, N. A.; Walba, D. M.; Bowman, C. N. *Chem. Mater.* **1998**, *10*, 2378.

(11) Broer, D. J.; Mol, G. N.; Challa, G. *Polymer* **1991**, *32*, 690.

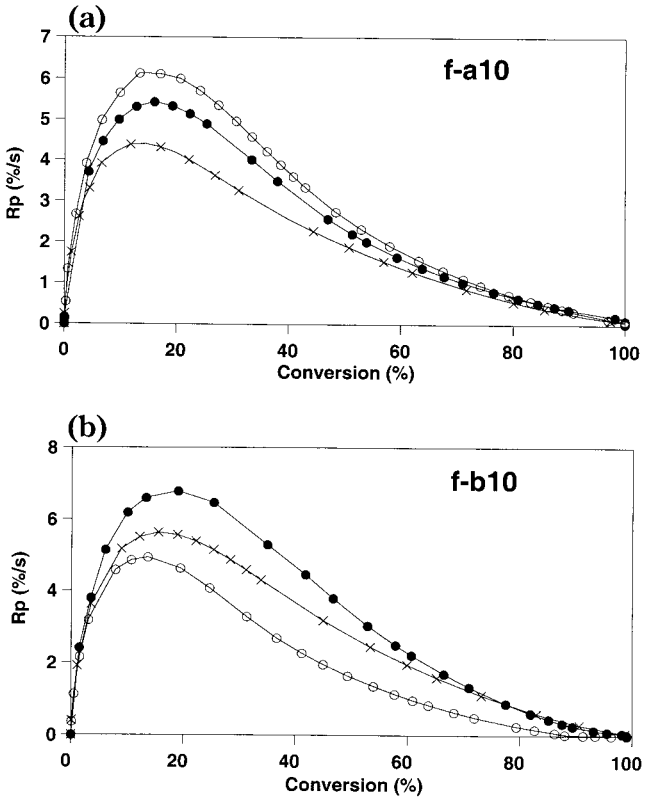

Figure 4. (a) Polymerization rate vs conversion for the samples **f-a10**, photopolymerized in the SmA phase (120 °C) [×], SmC* phase (103 °C) [○], and SmC*$_A$ phase (80 °C) [●]. (b) Polymerization rate vs conversion for the samples **f-b10**, photopolymerized in the SmA phase (120 °C) [×], SmC* phase (103 °C) [○], and SmC*$_A$ phase (80 °C) [●].

macroscopic order. The second gel was polymerized in the SmA phase without the application of an electric field.

The majority of the texture changes observed under the polarizing microscope when the gels were confined in either the nonaligned or the aligned cells were of little use for characterization purposes. Thus, the phase transition sequences were mainly determined by dielectric spectroscopy, switching experiments, and DSC measurements.

A phase sequence was determined for the three gels **g/f-b2**, regardless of the photopolymerization conditions: I 131.9 °C SmA 121 °C SmC* 108 °C ferri-SmC$_A$* 36.5 °C SmI* −4.5 °C K. Although this thermal behavior is rather similar to that determined for pure compound **f** (see Table 1), some differences are evident. Thus, the SmC*$_\alpha$ phase does not occur in the gels and, in addition, the transition from the SmC* to the SmC*$_A$ phase in the gels takes place over several degrees, a range in which phase coexistence is possible. The coexistence of the ferro- and antiferroelectric phases also occurs in pure compound **f** and this phenomenon depends on the sample thickness, as we shall discuss below.

The most interesting results were observed for the systems with low levels of cross-linking, and thus a more detailed description of these materials will be considered in this report.

To establish suitable comparisons, we will first consider pure compound **f**. Figure 5 shows the dielectric permittivity versus temperature relationship for **f** found upon cooling the sample in fields of 125 Hz and 100 kHz.

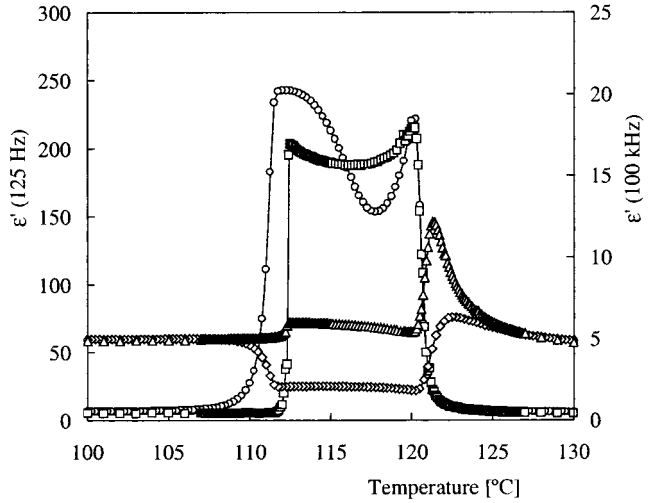

Figure 5. Real part of the dielectric permittivity vs tempertaure (upon cooling) at 125 Hz and 100 kHz for the pure compound **f** in cells of 7.5 and 50 μm. [○] 7.5 μm and 125 Hz; [□] 7.5 μm and 100 kHz; [◇] 50 μm and 125 Hz; [△] 50 μm and 100 kHz.

The SmC* phase is characterized by the high value of the dielectric permittivity, which is due to the contribution of the Goldstone mode. We plotted the results for **f** obtained using the Linkam cells (ITO-coated glass, thickness 7.5 μm) and the metallic cells (thickness 50 μm). The low-frequency permittivity in the ferroelectric phase shows typical behavior that is similar to other compounds with the same phase transition sequence: a peak inside the mesophase followed by a decrease and a further increase prior to the phase transition to a ferri- or antiferroelectric phase.[12,13] The origin of this behavior is not very clear but we believe that it could be related to changes in the pitch. (Under the polarizing microscope many dechiralization lines can be observed.) Moreover, the behavior of this compound is not totally ferrielectric, but shows some ferroelectric character that becomes more pronounced in the low-temperature range.[14] The region where the permittivity sharply decreases would correspond to the ferrielectric phase. However, the criterion is not clear because the behavior seems to be not purely ferrielectric but rather a phase coexistence of ferroelectric and antiferroelectric phases. Moreover, in Figure 5 one can clearly see that the dielectric behavior is different in the two types of cell. In the metallic cells there is a very sharp decrease in the permittivity that lasts no more than 0.5 °C, while in the Linkam cells the decrease lasts over a range of 4 °C. On the other hand, in the metallic cells the temperature range of the SmC* phase is shorter.

Figure 6 shows the dielectric permittivity versus temperature relationships upon cooling at 125 Hz for the three **g/f-b2** gels and compound **f** (Linkam cells). The permittivity behavior of the gels in the low-temperature zone of the high-permittivity range differs from that of compound **f**. The shape of the dependence has no minimum within the SmC* phase. Moreover, the

(12) de la Fuente, M. R.; Merino, S.; González, Y.; Ros, B.; Puértolas, J. A.; Castro, M. *Adv. Mater.* **1995**, *7*, 564.
(13) Bourny, V.; Pavel, J.; Lorman, V.; Nguyen, H. T. *Liq. Cryst.* **2000**, *27*, 559.
(14) Panarin, Y. P.; Kalinovskaya, O.; Vij, J. K.; Goodby, J. W. *Phys. Rev. E* **1997**, *55*, 4345.

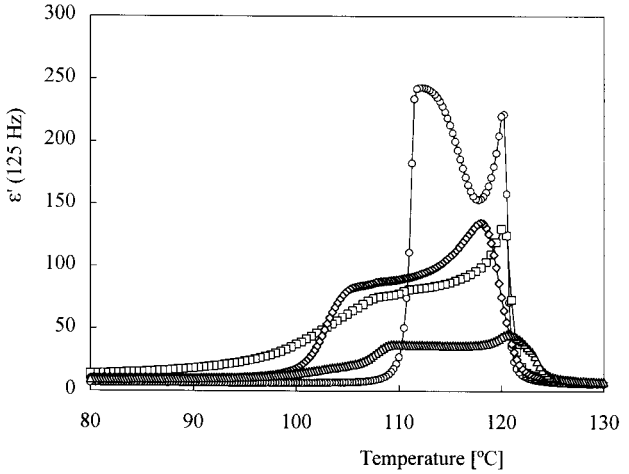

Figure 6. Real part of the dielectric permittivity vs temperature (upon cooling) at 125 Hz, cell thickness 7.5 μm. [○] **f**; [◇] **g/f-b2** photopolymerized in the SmA phase; [□] photopolymerized in the SmC*$_A$ phase without field; [△] photopolymerized in the SmC*$_A$ with field.

transition to the antiferroelectric SmC*$_A$ phase proceeds very slowly with a wide temperature range of phase coexistence (smooth decrease in the dielectric permittivity that starts at around 108 °C for all three gels). The starting point of the phase transition coincides with texture changes, which proceed gradually. However, if we applied a dc field or a triangular field strong enough to produce a reversal in the polarization, the transition to the antiferroelectric phase appeared very sharp.

From the dielectric data it can be inferred that the helicoidal structure of the SmC* phase is altered by the cross-linked network, with the effect being different for each gel. The Goldstone mode dielectric strength for the three gels is smaller than that for **f** and the frequency is greater (around 10^4 for **f** and around 5×10^4 for the gels). A nonchiral dopant tends to unwind the helix (increasing the pitch), producing a higher strength and a lower frequency. In our case, however, the contrary happens, indicating that the Goldstone mode is more affected by the presence of the network than by a lower chirality. It is probable that there is a proportion of the molecules, those very close to the network, that cannot participate in the process and do not contribute to the strength of the Goldstone mode. It is also interesting to note that the maximum value of the Goldstone mode strength occurs at the same temperature for pure compound **f** and the gel photopolymerized in the SmC*$_A$; however, for the gel photopolymerized in the SmA phase the Goldstone maximum occurs at a lower temperature and for the gel photopolymerized in the SmC*$_A$ phase with field at a higher temperature. It is probable that this trend is also due to the network. For example, in the gel photopolymerized in the SmA phase, the strands formed by the polymer point along the smectic layer normal; a proportion of the molecules also tend to be normal to the smectic layers despite the material being in the SmC* phase and we will return to this point later. On the other hand, the Goldstone mode frequency is directly related to the (ferroelectric) switching time. It is not the only factor that determines the value of the switching time but a high value for this frequency opens up the possibility of having gels with switching times that are no slower than that of the pure AFLC.

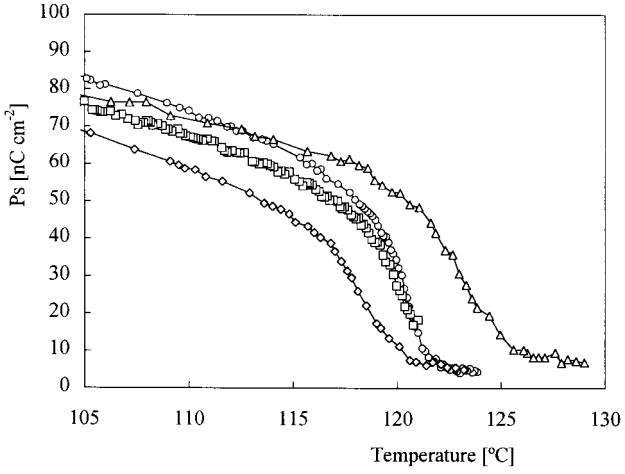

Figure 7. Spontaneous polarization vs temperature. [○] **f**; [◇] **g/f-b2** photopolymerized in the SmA phase; [□] **g/f-b2** photopolymerized in the SmC*$_A$ phase without field; [△] **g/f-b2** photopolymerized in the SmC*$_A$ with field.

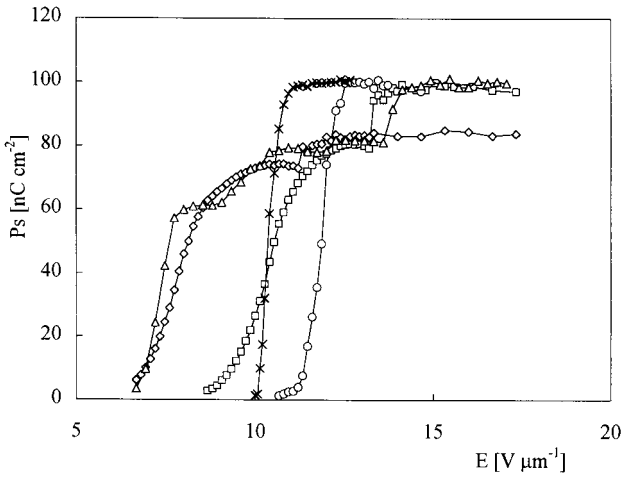

Figure 8. Spontaneous polarization vs the amplitude of the applied triangular field at 90 °C in the SmC*$_A$ phase. [○] **f**; [◇] **g/f-b2** photopolymerized in the SmA phase; [□] **g/f-b2** photopolymerized in the SmC*$_A$ phase without field; [△] **g/f-b2** photopolymerized in the SmC*$_A$ with field; [×] **g/f-c2** photopolymerized in the SmC*$_A$ phase without field.

More information regarding the influence of the photoreaction conditions on the anisotropic environment of the host molecules **f** can be obtained from the electrooptic study presented below. Figure 7 shows the relationship between spontaneous polarization (P_S) and temperature, obtained by applying a triangular field of 50 Hz to 7.5-μm cells containing **f** and each of the three gels **g/f-b2**. The amplitude of the applied field was sufficient to reach the saturation value over all the temperature range. In the case of antiferroelectric or ferrielectric phases the field should be sufficient to promote the switching to the ferroelectric synclinic structure. Results show that pure **f** has slightly higher P_S values than the gels **g/f-b2**, which were photopolymerized in the antiferroelectric phase. For the sample photopolymerized in the SmA phase the values are lower. The reason for this behavior could be the same as that described above: a proportion of the molecules in the latter gel tends to point in a direction normal to the smectic layers and hence do not participate in the switching process. The high value of the spontaneus

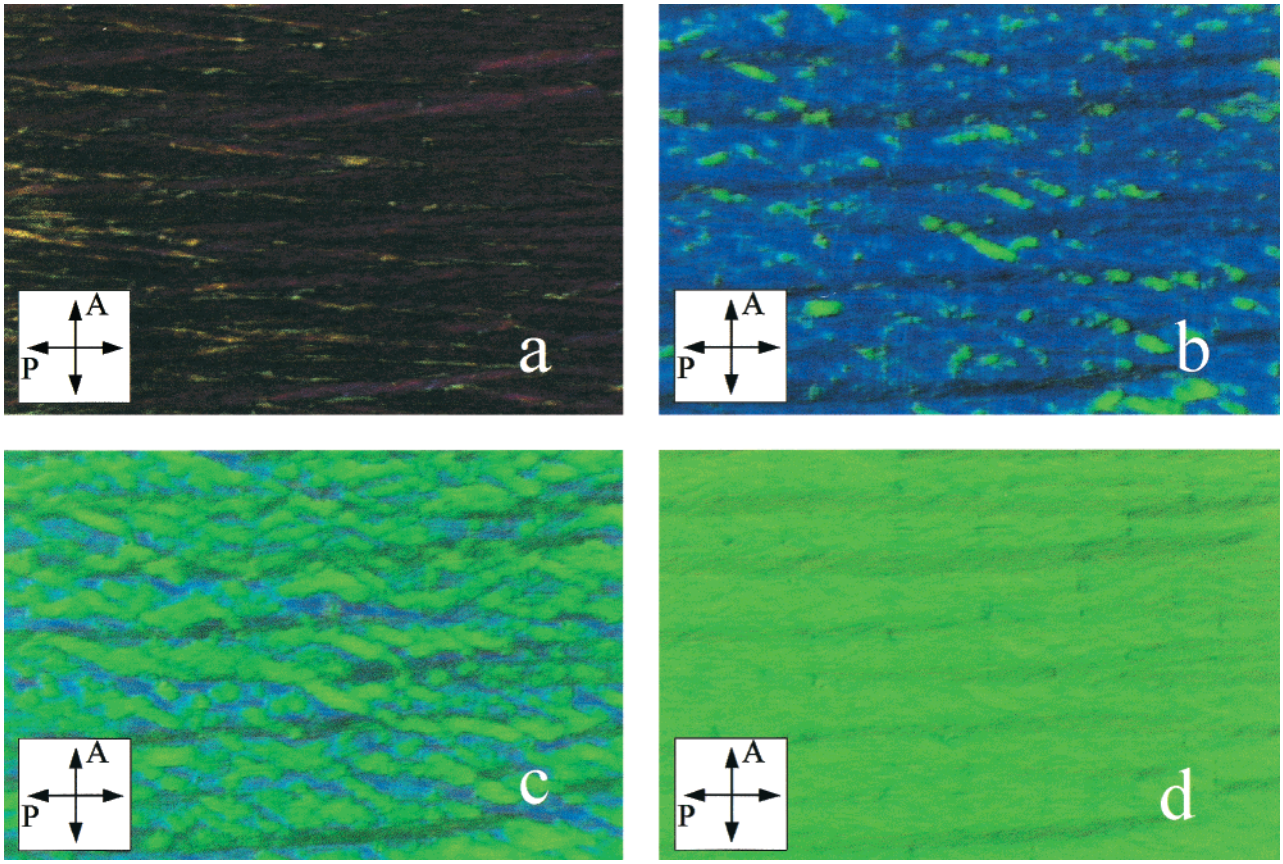

Figure 9. Textures of the gel **g/f-b2** at 90 °C in the SmC^*_A phase under the polarizing microscope. The direction of the rubbing coincides with the polarizer and the layer normal with the analyzer: (a) no field, dark state; (b) at 5 V μm^{-1}; (c) at 7 V μm^{-1}; (d) at 9 V μm^{-1}, bright state.

polarization observed for the gels and even for the compound **f** that is deep into the SmA phase is due to the high field used to measure.

Figure 8 shows a plot of P_S versus the amplitude of the applied triangular field at 90 °C for the three gels **g/f-b2** and the gel **g/f−c2**. All samples show antiferroelectric behavior and the presence of a threshold field, with this critical field being smaller for the gels. For **f** and the gel **g/f-c2** the polarization jumps from zero to the saturation value in a single step. The other gels go through intermediate steps of increasing polarization. This fact points to the presence of network-induced domains, with different critical fields, a combination of which produces the observed global effect. Microscopic observation of the cells between crossed polarizers during the application of fields of increasing bias confirmed the presence of domains that remain in different states at intermediate voltages. Figure 9 shows photographs of the gel photopolymerized in the SmC^*_A phase without an applied field, as observed under the polarizing microscope. The dark state with no field occurs when polarizer or analyzer are in the direction of the layer normal (optical axis) (Figure 9a). The bright state, Figure 9d, corresponds to one of the ferroelectric states produced by the field. For intermediate field values there are several domains with intermediate transmittances that occur because there are simultaneously regions in the ferroelectric state and others that remain unswitched in the antiferroelectric state (Figure 9b,c). For the gel **g/f-c2** the behavior is similar to that of pure compound **f**. As in other antiferroelectric compounds the switching takes place through "fingers" that grow along the smectic layers.

Of particular interest is the behavior of the gel photopolymerized in the SmC^*_A phase with field. Figure 10a shows the polarization current versus field plot for two different maximum values of the triangular field (equal frequency). The cycles are asymmetric in that the behavior for the positive slope is different from that for the negative slope. In other words, the dynamics of the transition $F^- \rightarrow AF \rightarrow F^+$ are not the same as those for $F^+ \rightarrow AF \rightarrow F^-$, where F^+ and F^- account for the two ferroelectric states and AF for the antiferroelectric one. After integration of both branches for different amplitude values of the triangular field, we obtained the results shown in Figure 10b. The same asymmetry appears in the electro-optic cycles, that is, in the field dependence of the optical transmittance, and this will be discussed in more detail later.

Parts a−c of Figure 11, respectively, show the electro-optic hysteresis cycles at 90 °C of pure **f**, the gel photopolymerized in the SmC^*_A without field, and the gel photopolymerized in the SmC^*_A phase with field. Parts a and b of Figure 11 both show typical tristable antiferroelectric switching, although the contrast for the gel is somewhat smaller. In accordance with the results for the spontaneous polarization, the critical field is smaller for the gel. Other authors have described how the slope of the switching from the AF state to any one of the F states becomes smaller for gels.[15] However, we did not observe this phenomenon, although the slope of the relaxation $F \rightarrow AF$ is smaller, as is the hysteresis.

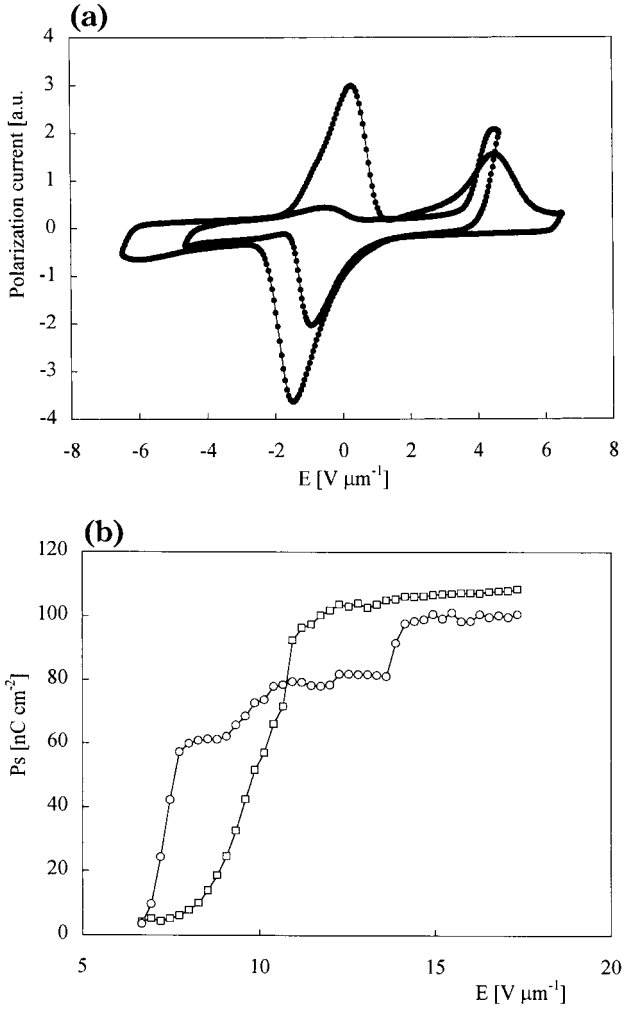

Figure 10. (a) Polarization current vs field (triangular wave, 50 Hz) for two different amplitudes of the field. At 90 °C in the SmC*$_A$ phase for the gel **g/f-b2** photopolymerized in the SmC*$_A$ phase with field. (b) Spontaneous polarization vs the amplitude of the applied triangular field at 90 °C in the SmC*$_A$ phase for the gel **g/f-b2** photopolymerized in the SmC*$_A$ phase with field: [○] integrating the branch with positive slope; [□] integrating the branch with negative slope.

This situation indicates that the structure adopted by the network as a consequence of the conditions in which it was created influences the behavior of the host molecules. The gel, which was photopolymerized in the absence of an electric field in the SmC*$_A$ phase, adopted the herringbone structure typical of this phase. For this reason the gel favors the relaxation of the host molecules from a synclinic arrangement to an anticlinic one under applied fields at which the AFLC molecules by themselves would not relax.

The effect of the network is even more important for the gel represented in Figure 11c. In this case one of the ferroelectric states involved in the switching process is not stable and tends to relax, even at high applied voltages. From the asymmetry of the switching process it is evident that the polymeric network has adopted such a structure that one of the synclinic arrangements

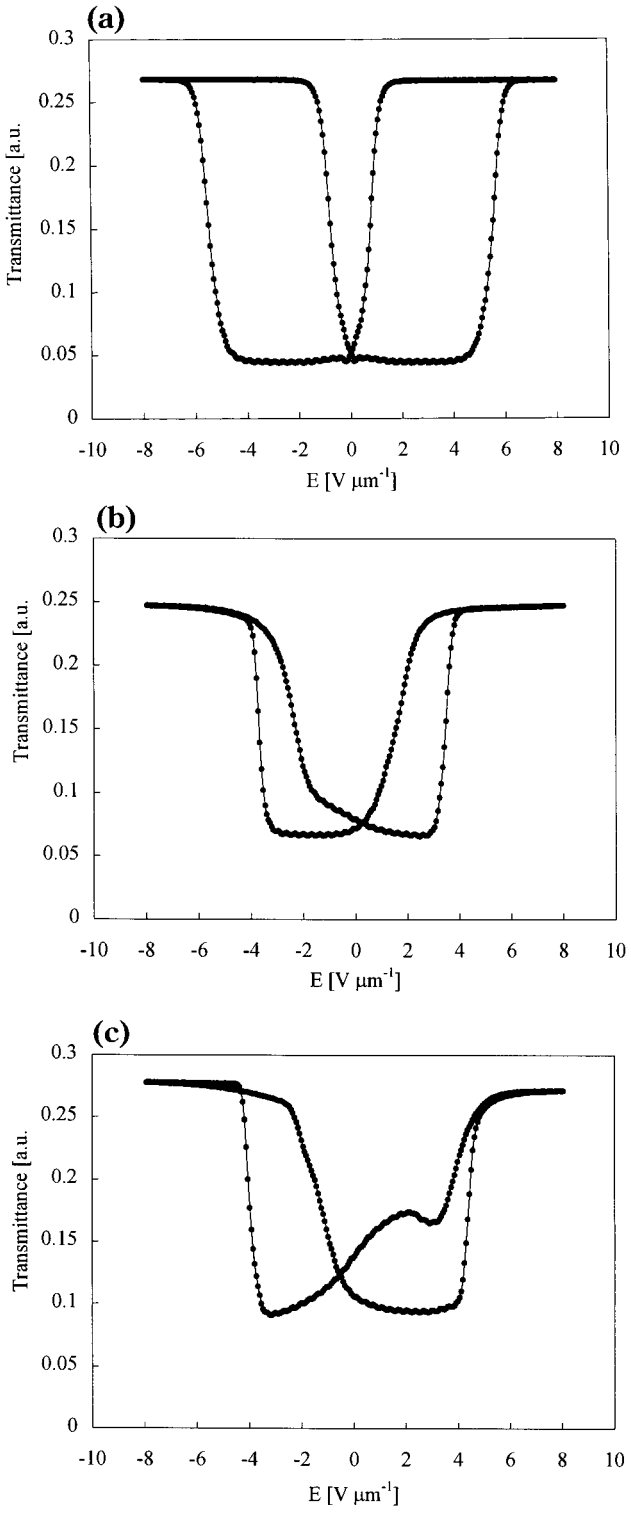

Figure 11. Transmittance vs field (triangular wave, 0.5 Hz) at 90 °C in the SmC*$_A$ phase. (a) **f**; (b) **g/f-b2** photopolymerized in the SmC*$_A$ phase without field; (c) **g/f-b2** photopolymerized in the SmC*$_A$ phase with field.

is favored over the other. This point has been extensively treated in ref 15c.

Another important point is that in pure **f** (and in the gel **g/f-c2**) the switching proceeds from the dark (off antiferroelectric) to the bright (on ferroelectric) state by nucleation of fingers parallel to the smectic layers, while in the other gels the nucleation of domains is similar to that shown in Figure 9.

(15) (a) Strauss, J.; Kitzerow, H.-S. *Appl. Phys. Lett.* **1996**, *69*, 725. (b) Strauss, J.; Kitzerow, H.-S. *Ber. Bunsen-Ges. Phys. Chem.* **1998**, *102*, 1609. (c) Glossmann, J.; Hoischen, A.; Röder, T.; Kitzerow, H.-S. *Ferroelectrics* **2000**, *243*, 95.

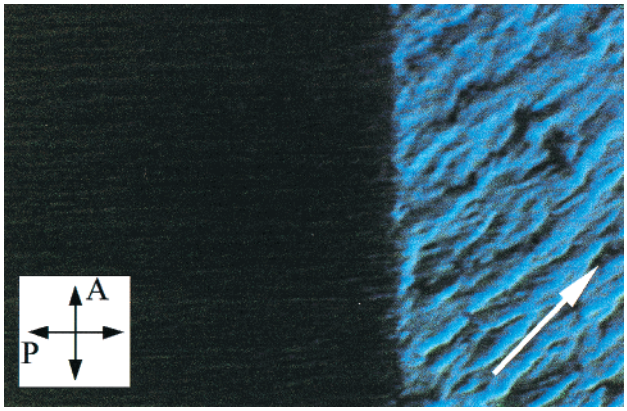

Figure 12. Textures of the gel **g/f-b2** photopolymerized in the SmC^*_A phase with field at a temperature above the clearing point of the pure compound **f**, showing some birefringence with the electrode area in extinction position.

Finally, we present the analysis of the microscopic textures of the samples in the isotropic phase, that is, at temperatures above the clearing point of the AFLC **f** (see Figure 12). This analysis gives information about the polymer network formed in the gels. The network induces some birefringence due to the fact that a small number of the AFLC molecules remain oriented.

The most interesting result was obtained for the gel photopolymerized during the application of an electric field in the SmC^*_A phase. In this case, the textures in regions of the cell in the presence and absence of electrode are different. The application of an electric field during the polymerization has shifted the optical axis of the system with respect to the alignment direction induced by the surface conditions. The network freezes the order characteristic of the conditions under which the polymerization took place (synclinic in our case). This means that the extinction conditions between crossed polarizers in the regions with electrode (where the field was actually applied) differ from those needed for extinction in the regions without electrode in which the order favored by the network is anticlinic. This effect has been pointed out as being applicable for optical storage.

As far as the influence of the chemical structure of the network is concerned, networks obtained from **b** (with very similar behavior to that of the network from **a**) show behavior that is very different from that observed for the gel based on compound **c**. Gel **g/f-c2** shows dielectric and electro-optical responses very close to the processes observed for the pure material **f**. Nevertheless, it is important to note that a cell containing this gel was still perfectly aligned, even after storage for 1 year. This is not the case for compound **f**.

The differences due to the diacrylate used to generate the anisotropic network may be attributed to the surface conditions of the liquid crystal. This effect appears as a consequence of polar interactions, which will be stronger between the aromatic central cores of **f** and **a** or **b**. Thus, the initial monomer distribution[10] and the network morphology should also be considered.[16,17] SEM experiments must be carried out to confirm this model, although morphological differences in this area have been reported in the literature.[17]

(16) Hikmet, R. A. M.; Boots, H. M. J. *Phys. Rev. E* **1995**, *51*, 5824.

The influence of the polymer concentration on the electro-optic response of antiferroelectric gels has been previously studied by Kitzerow et al. (up to 20 wt %).[15] In our case, 10 mol % of the network proved to be unsuitable for practical purposes. These materials exhibit a switching process closer to ferroelectric materials with transmission at $V = 0$.

Conclusions

The antiferroelectric properties of gels obtained by in situ photopolymerization of mixtures of an antiferroelectric compound, **f**, and three cross-linkers, **a**, **b**, and **c**, have been investigated. Although the properties of these materials are not very different with respect to the pure compound, at least if the percentage of the cross-linker is 2% or less, the stabilization effect is quite important. The alignment of the gels is preserved during prolonged storage without any damage (more than 1 year). The orientational order of the mesophase in which the photopolymerization occurs is transferred to the polymer network, a situation that has a great influence on some of the properties. The network could consist of strands embedded in the liquid crystal that interact elastically with the mesogenic molecules. Thus, the electro-optical properties could be controlled by the orientation of the network. This was clearly demonstrated for the gels photopolymerized in the antiferroelectric phase with a bias field. One of the ferroelectric states is more stable than the other. In the same way, we can explain the effect on the magnitude of the spontaneous polarization and Goldstone mode strength. When photopolymerization occurs in the orthogonal SmA phase, a proportion of the molecules tend to lie along the normal to the smectic layers, even in the tilted phases, and hence do not contribute to the switching processes.

Experimental Section

Synthesis of the Compounds. The synthetic pathways to obtain the cross-linkers **a** and **b** and the AFLC **f** are depicted in Schemes 1, 2, and 3. Compound **c** was commercially available from Aldrich. Organic starting chemicals were purchased from Aldrich or Lancaster and used as delivered.

*(a) Synthesis of Cross-linker **a**. Methyl 4-(11′-Hydroxyundecyloxy)benzoate **1**.* A mixture of methyl 4-hydroxybenzoate (5.00 g, 32.86 mmol), 11-bromoundecanol (8.26 g, 32.86 mmol), and potassium carbonate (9.08 g, 65.70 mmol) in dry dimethylformamide (250 mL) was heated under reflux for 4 h. The reaction mixture was allowed to cool to room temperature. Water (80 mL) was added and the aqueous phase was extracted with ether (3×). The combined organic layers were washed twice with water after with 2 M NaOH and finally dried over $MgSO_4$. The product was collected by filtration as a white solid and used in the next step without further purification. Yield: quantitative. R_f (1:1 hexane/ethyl acetate): 0.56. ^{1}H NMR (300 MHz, $CDCl_3$) δ: 1.20−1.60 (m, 16H), 1.72−1.82 (m, 2H), 3.58−3.65 (m, 2H), 3.86 (s, 3H), 3.98 (t, J = 6.5 Hz, 2H), 6.87 (d, J = 9.0 Hz, 2H), 7.95 (d, J = 9.0 Hz, 2H). IR (NaCl) ν_{max}/cm^{-1}: 3500−3100, 1722, 1608, 1462, 1259, 1110, 1020, 698.

(17) (a) Fung, Y. K.; Yang, D. K.; Ying, S.; Chien, L. C.; Zimer, S.; Doane, J. W. *Liq. Cryst.* **1995**, *19*, 797. (b) Rajaram, C. V.; Hudson, S. D.; Chien, L. C. *Chem. Mater.* **1995**, *7*, 2300. (c) Rajaram, C. V.; Hudson, S. D.; Chien, L. C. *Chem. Mater.* **1996**, *8*, 2451. (d) Dierking, I.; Kosbar, L. L.; Afzali-Ardakani, A.; Lowe, A. C.; Held, G. A. *Appl. Phys. Lett.* **1997**, *71*, 2454.

4-(11′-Hydroxyundecyloxy)benzoic Acid ***2***. LiOH·H_2O (2.16 g, 51.50 mmol) was added in small portions to a suspension of methyl 4-(11′-hydroxyundecyloxy)benzoate (4.00 g, 12.41 mmol) in methanol (100 mL) and water (35 mL) at 0 °C. The reaction mixture was refluxed for 2 h and allowed to cool to room temperature. Then, 3.5% aqueous NaOH (150 mL) was added, followed by concentrated HCl. The product was collected by filtration and recrystallized from ethanol/water (1:1). White solid. Yield from methyl 4-hydroxybenzoate: 8.00 g (79%). mp: C 105 °C, SmC 120 °C, SmA 135 °C, I. 112 °C. R_f (1:1 hexane/ethyl acetate): 0.32. ^{1}H NMR (300 MHz, DMSO-d_6) δ: 1.15−1.40 (m, 16H), 1.65−1.75 (m, 2H), 3.33 (t, J = 6.4 Hz, 2H), 3.98 (t, J = 6.5 Hz, 2H), 4.30 (broad s, 1H), 6.96 (d, J = 8.9 Hz, 2H), 7.82 (d, J = 8.9 Hz, 2H), 12.6 (broad s, 1H). IR (NaCl) ν_{max}/cm^{-1}: 3550−3300, 1698, 1632, 1452, 1335, 1275, 1190, 1068, 870, 790.

4-(11′-Acryloyloxyundecyloxy)benzoic Acid ***3***. Freshly distilled acryloyl chloride (0.70 g, 7.78 mmol) was added dropwise to a solution of 4-(11′-hydroxyundecyloxy)benzoic acid (2.00 g, 6.48 mmol), *N*,*N*-dimethylaniline (0.94 g, 1.00 mL, 7.78 mmol), and 2,6-di-*tert*-butyl-4-methylphenol (catalytic amount) in dry dioxane (10 mL) at 50 °C under nitrogen. The reaction mixture was stirred at this temperature for 2 h, allowed to cool to room temperature, and poured into a solution of concentrated HCl (0.2 mL) in water (43 mL) and ice (10 g). The product was collected by filtration and recrystallized from 2-propanol. Yield: 1.60 g (79%). mp: C 105 °C, SmC 120 °C, SmA 135 °C, I. 101 °C. R_f (ethyl acetate): 0.61. ^{1}H NMR (300 MHz, DMSO-d_6) δ: 1.18−1.25 (m, 14H), 1.50−1.62 (m, 2H), 1.62−1.78 (m, 2H), 4.01 (t, J = 6.5 Hz, 2H), 4.07 (t, J = 6.6 Hz, 2H), 5.91 (dd, J = 10.4 Hz, J = 1.6 Hz, 1H), 6.21 (dd, J = 17.3 Hz, J = 10.4 Hz, 1H), 6.27 (dd, J = 17.3 Hz, J = 1.6 Hz, 1H), 7.00 (d, J = 9.0 Hz, 2H), 7.85 (d, J = 9.0 Hz, 2H). IR (NaCl) ν_{max}/cm^{-1}: 3300−2500, 1720, 1678, 1604, 1292, 1261, 1209, 1170, 1012.

4-[11′-(3″-Chloropropionyloxy)undecyloxy]benzoic Acid ***4***. 3-Chloropropionyl chloride (2.47 g, 19.45 mmol) was added slowly to a solution of 4-(11′-hydroxyundecyloxy)benzoic acid (5.00 g, 16.21 mmol) in dry dichloromethane (25 mL) under nitrogen. The reaction mixture was refluxed for 3 h and allowed to cool to room temperature. Water (20 mL) was added, the organic phase separated, and the aqueous phase extracted into dichloromethane (2×). The combined organic layers were washed with 2% NaOH, followed by water. The solvent was evaporated in vacuo and the crude material purified by column chromatography (silica gel, dichloromethane) and recrystallized from hexane/ethanol (7:3). Yield: 1.96 g (30%). mp: C 105 °C, SmC 120 °C, SmA 135 °C, I. 109 °C. R_f (9:1 dichloromethane/ethyl acetate): 0.48. ^{1}H NMR (300 MHz, $CDCl_3$) δ: 1.18−1.50 (m, 14H), 1.55−1.68 (m, 2H), 1.70−1.85 (m, 2H), 2.76 (t, J = 6.6 Hz, 2H), 3.73 (t, J = 6.6 Hz, 2H), 4.00 (t, J = 6.7 Hz, 2H), 4.10 (t, J = 6.6 Hz, 2H), 6.90 (d, J = 9.0 Hz, 2H), 8.02 (d, J = 9.0 Hz, 2H). IR (NaCl) ν_{max}/cm^{-1}: 3400−2400, 1738, 1683, 1609, 1256, 1175, 849, 774, 647.

*1,4-Phenyl Bis[4-(11′-acryloyloxyundecyloxy)benzoate] (****a****). Method I*. Oxalyl chloride (1.86 g, 14.7 mmol) was added dropwise to a suspension of 4-(11′-acryloyloxyundecyloxy)-benzoic acid (1.75 g, 4.90 mmol), 2,6-di-*tert*-butyl-4-methylphenol (catalytic amount), and dimethylformamide (5 drops) in dry dichloromethane (40 mL) under nitrogen. The reaction mixture was stirred at room temperature for 24 h. The solvent and excess oxalyl chloride were removed under reduced pressure and the yellow oil obtained was used in the next step without further purification. IR (NaCl) ν_{max}/cm^{-1}: 1845, 1800, 1680, 1540, 1485, 1340, 1240, 1110, 950.

A solution of 4-(11-acryloyloxy)undecyloxybenzoyl chloride (4.90 mmol) in dry THF (10 mL) was added dropwise to a solution of hydroquinone (270 mg, 2.45 mmol), triethylamine (0.64 g, 0.89 mL, 6.37 mmol), and 2,6-di-*tert*-butyl-4-methylphenol (catalytic amount) in dry THF (25 mL) under nitrogen. The mixture was stirred at room temperature for 24 h. Ether was added and the organic phase was washed with saturated aqueous $NaHCO_3$ after with water (3×) and finally dried over $MgSO_4$. The solvent was evaporated in vacuo and the crude product purified by column chromatography (silica gel, dichloromethane) and recrystallized from 2-propanol (twice). Yield: 1.66 g (85%).

Method II. 4-[11′-(3″-Chloropropionate)]undecyloxybenzoyl chloride was prepared in a similar way to that described for the preparation of 4-(11-acryloyloxy)undecyloxybenzoyl chloride, using the following quantities: 4-[11′-(3"-Chloropropionyloxy)]undecyloxybenzoic acid (3.50 g, 8.80 mmol) and oxalyl chloride (1.57 g, 13.20 mmol). IR (NaCl) ν_{max}/cm^{-1}: 1772, 1741, 1602, 1267, 1212, 1168, 879, 841.

A solution of 4-[11′-(3″-chloropropionate)]undecyloxybenzoyl chloride (8.80 mmol) in dry dichloromethane (10 mL) was added slowly to a solution of hydroquinone (484 mg, 4.40 mmol), triethylamine (1.42 g, 14.08 mmol), and 2,6-di-*tert*-butyl-4-methylphenol (catalytic amount) in dry dichloromethane (30 mL) under nitrogen. The reaction mixture was stirred for 24 h under nitrogen. Triethylamine (1.78 g, 17.6 mmol) was added and the mixture refluxed for 15 h with protection from light. The reaction mixture was washed with saturated aqueous $NaHCO_3$ after with water (3×) and finally dried over $MgSO_4$. The crude product was purified by column chromatography (silica, hexane/dichloromethane 1:4) and recrystallized from ethanol (twice). Yield: 5.95 g (85%). R_f (dichloromethane): 0.26. ^{1}H NMR (300 MHz, $CDCl_3$) δ: 1.20−1.50 (m, 28H), 1.55−1.65 (m, 4H), 1.70−1.85 (m, 4H), 4.02 (t, J = 6.5 Hz, 4H), 4.13 (t, J = 6.6 Hz, 4H), 5.79 (dd, J = 10.4 Hz, J = 1.5 Hz, 2H), 6.10 (dd, J = 17.3 Hz, J = 10.4 Hz, 2H), 6.38 (dd, J = 17.3 Hz, J = 1.5 Hz, 2H), 6.96 (dd, J = 9.0 Hz, J = 2.6 Hz, 4H), 7.24 (s, 4H), 8.12 (dd, J = 9.0 Hz, J = 2.6 Hz, 4H). ^{13}C NMR (300 MHz, $CDCl_3$): 166.4, 164.9, 163.6, 148.4, 132.3, 130.4, 128.6, 122.6, 121.4, 114.3, 68.3, 64.7, 29.5, 29.3, 29.2, 29.1, 28.6, 26.0, 25.9. IR (NaCl) ν_{max}/cm^{-1}: 1728, 1716, 1604, 1254, 1207, 1161, 1074, 966, 847. MS FAB+ *m*/*z*: 121, 154, 189, 273, 345. Calcd. for $C_{48}H_{62}O_{10}$: C, 72.16; H, 7.82. Found: C, 72.25; H, 7.80.

(b) Synthesis of Cross-linker ***b***. *Methyl 4′-Hydroxy-4-biphenylcarboxylate* ***5***. Concentrated H_2SO_4 (9.4 mL) was added slowly to a solution of 4′-hydroxy-4-biphenylcarboxylic acid (10.00 g, 46.7 mmol) in methanol (375 mL). The reaction mixture was heated under gentle reflux for 4 h and then allowed to cool to room temperature. The solvent was partially removed in vacuo and water (200 mL) added. The precipitate was collected by filtration and washed with water. The product was recrystallized from ethanol to give white needles. Yield: 8.33 g (78%). mp: C 105 °C, SmC 120 °C, SmA 135 °C, I. 229 °C. R_f (1:1 hexane/ethyl acetate): 0.64. ^{1}H NMR (300 MHz, $CDCl_3$) δ: 3.92 (s, 3H), 4.85 (s, 1H), 6.90 (d, J = 8.6 Hz, 2H), 7.50 (d, J = 8.6 Hz, 2H), 7.58 (d, J = 8.4 Hz, 2H), 8.05 (d, J = 8.4 Hz, 2H). IR (NaCl) ν_{max}/cm^{-1}: 3400, 1690, 1585, 1430, 1200.

10-Undecenyl 4-Toluenesulfonate ***6***. To a solution of tosyl chloride (20.15 g, 0.106 mol) in dry pyridine (18 mL) at −10 °C under nitrogen was added 10-undecene-1-ol (17.7 mL, 0.088 mol) dropwise so that the temperature did not exceed 5 °C. After the addition was complete, the reaction mixture was stirred for 2 h at 0 °C. Water/ice (18 mL) was added, followed by a solution of concentrated HCl (10.6 mL) in water/ice (18 mL). The mixture was extracted into ether (3×) and the combined organic layers were washed with brine and dried over $MgSO_4$. Concentration in vacuo and filtration through silica gel (dichloromethane) gave the product as a colorless oil. Yield: 27.94 g (98%). R_f (dichloromethane): 0.98. ^{1}H NMR (300 MHz, $CDCl_3$) δ: 1.10−1.35 (m, 12H), 1.55−1.65 (m, 2H), 1.95−2.05 (m, 2H), 2.42 (s, 3H), 3.99 (t, J = 6.5 Hz, 2H), 4.90−5.00 (m, 2H), 5.70−5.85 (m, 1H), 7.32 (d, J = 8.4 Hz, 2H), 7.76 (d, J = 8.4 Hz, 2H). IR (film) ν_{max}/cm^{-1}: 2925, 2850, 1600, 1360, 1190, 1175, 1100, 950, 910, 815.

4′-(10″-undecenyloxy)-4-biphenylcarboxylic Acid ***7***. A mixture of methyl 4′-hydroxy-4-biphenylcarboxylate (3.80 g, 16.65 mmol) and KOH (1.07 g, 19.15 mmol) in ethanol (25 mL) was stirred at room temperature for 1 h. A solution of 10-undecenyl 4-toluenesulfonate (5.40 g, 16.65 mmol) in ethanol (5 mL) was then added and the mixture heated under reflux for 28 h. After this time, a solution of KOH (2.80 g) in water (20 mL) was added slowly to the vigorously stirred reaction mixture. The mixture was refluxed for 1 h and then allowed to cool. The precipitate was collected by filtration and added to a mixture

of ethanol (40 mL) and water (10 mL). The resulting mixture was refluxed for 2 h and allowed to cool to room temperature. The precipitate was collected by filtration, washed with water, and recrystallized from ethanol. White solid. Yield: 4.60 g (75%). mp: C 105 °C, SmC 120 °C, SmA 135 °C, I. 159 °C. R_f (9:1 dichloromethane/ethyl acetate): 0.15. ^{1}H NMR (300 MHz, DMSO-d_6) δ: 1.20−1.45 (m, 12H), 1.65−1.80 (m, 2H), 1.90−2.00 (m, 2H), 3.91 (t, J = 6.6 Hz, 2H), 4.80−4.90 (m, 2H), 5.60−5.80 (m, 1H), 6.88 (d, J = 8.6 Hz, 2H), 7.47 (d, J = 8.6 Hz, 2H), 7.52 (d, J = 8.2 Hz, 2H), 7.95 (d, J = 8.2 Hz, 2H). IR (NaCl) ν_{max}/cm^{-1}: 3300−2500, 1684, 1605, 1464, 1435, 1290, 913, 835, 773.

10-Undecenyl 4-Hydroxybenzoate ***8***. A mixture of 4-hydroxybenzoic acid (2.35 g, 17.00 mmol) and $NaHCO_3$ (1.43 g, 17.00 mmol) in dimethylacetamide (DMAC) (15 mL) was heated under reflux until the formation of CO_2 had ceased (3 h). A solution of 10-undecenyl 4-toluenesulfonate (5.51 g, 17.00 mmol) in DMAC (2 mL) was then added. The mixture was refluxed for an additional 1 h, poured into water, and extracted into dichloromethane (3×). The combined organic phases were washed with saturated aqueous $NaHCO_3$ (2×) after with water and finally dried over $MgSO_4$. The solvent was evaporated in vacuo and the crude product purified by column chromatography (silica gel, hexane/ethyl acetate 95:5). Pale yellow oil. Yield: 3.31 g (67%). R_f (dichloromethane): 0.31. ^{1}H NMR (300 MHz, $CDCl_3$) δ: 1.20−1.45 (m, 12H), 1.70−1.80 (m, 2H), 2.00−2.10 (m, 2H), 4.26 (t, J = 6.6 Hz, 2H), 4.85−5.00 (m, 2H), 5.80 (s, 1H), 5.70−5.85 (m, 1H), 6.85 (d, J = 8.8 Hz, 2H), 7.94 (d, J = 8.8 Hz, 2H). IR (film) ν_{max}/cm^{-1}: 3500−3000, 1682, 1608, 1591, 1280, 1165, 910, 850, 773.

10″-Undecenyl 4-[4′-(10-Undecenyloxy)biphenoyloxy]benzoate ***9***. *N*,*N*-Dicyclohexylcarbodiimide (2.31 g, 11.19 mmol) was added to a solution of 4′-(10″-undecenyloxy)-4-biphenylcarboxylic acid (3.16 g, 8.61 mmol), 10-undecenyl 4-hydroxybenzoate (2.50 g, 8.61 mmol), and *N*,*N*-(dimethylamino)pyridine (0.158 g, 1.29 mmol) in dry dichloromethane (80 mL) at room temperature under nitrogen. The reaction mixture was stirred for 24 h at room temperature and then filtered through silica gel. The solvent was removed in vacuo and the crude product purified by recrystallization from ethanol. Yield: 3.74 g (68%). mp: K 79 °C SmC 140 °C SmA 162 °C I. R_f (dichloromethane): 0.75. ^{1}H NMR (300 MHz, $CDCl_3$) δ: 1.20−1.50 (m, 24H), 1.70−1.85 (m, 4H), 2.00−2.10 (m, 4H), 4.00 (t, J = 6.6 Hz, 2H), 4.31 (t, J = 6.6 Hz, 2H), 4.00−5.00 (m, 4H), 5.70−5.85 (m, 2H), 6.98 (d, J = 8.9 Hz, 2H), 7.30 (d, J = 8.8 Hz, 2H), 7.58 (d, J = 8.9 Hz, 2H), 7.68 (d, J = 8.6 Hz, 2H), 8.12 (d, J = 8.8 Hz, 2H), 8.22 (d, J = 8.6 Hz, 2H). IR (NaCl) ν_{max}/cm^{-1}: 1737, 1710, 1462, 1375, 1285, 1270, 830, 760.

11″-Hydroxyundecyl 4-[4′-(11-Hydroxyundecyloxy)biphenoyloxy]benzoate ***10***. To a solution of compound **9** (3.10 g, 4.85 mmol) in dry THF under nitrogen was added 9-BBN in THF (0.5 M, 29.04 mL, 14.52 mmol). The mixture was stirred at room temperature for 3 h and, after this time, cooled to 0 °C. Ethanol (29.0 mL) and 30% hydrogen peroxide (9.9 mL, 87.3 mmol) were then added. The mixture was stirred at 0 °C for 1 h and poured into water with vigorous stirring. The precipitate was collected by filtration and washed with water followed by dichloromethane. Yield: 3.32 g (95%). mp: K 105 °C SmC 120 °C SmA 135 °C I. R_f (1:4 hexane/ethyl acetate): 0.40. ^{1}H NMR (300 MHz, CF_3CO_2D) δ: 1.30−2.00 (m, 36H), 3.93 (t, J = 6.6 Hz, 2H), 4.38 (t, J = 7.0 Hz, 2H), 4.50−4.60 (m, 3H), 7.23 (d, J = 8.8 Hz, 2H), 7.43 (d, J = 8.8 Hz, 2H), 7.73 (d, J = 8.8 Hz, 2H), 7.83 (d, J = 8.4 Hz, 2H), 8.28 (d, J = 8.8 Hz, 2H), 8.36 (d, J = 8.4 Hz, 2H). IR (NaCl) ν_{max}/cm^{-1}: 3390, 1735, 1710, 1600, 1460, 1375, 1280, 830, 760.

*11″-Acryloyloxyundecyl 4-[4′-(11-Acryloyloxyundecyloxy)biphenoyloxy]benzoate (****b****)*. A mixture of compound **10** (2.40 g, 3.56 mmol), triethylamine (1.07 g, 1.48 mL, 10.67 mmol), and 2,6-di-*tert*-butyl-4-methylphenol (catalytic amount) in dry THF (150 mL) under nitrogen was stirred at 60 °C for 1 h. A solution of freshly distilled acryloyl chloride (0.90 g, 0.81 mL, 9.96 mmol) in dry THF (10 mL) was added dropwise to the vigorously stirred reaction mixture. The reaction mixture was stirred at 60 °C for 24 h with protection from light, allowed to cool to room temperature, and poured into a solution of 10% aqueous NH_4Cl (250 mL). The mixture was extracted into dichloromethane (3×) and the combined organic phases were washed with water (2×) and dried over $MgSO_4$. The crude product was purified by column chromatography (silica gel, hexane/dichloromethane 1:3) and recrystallized from ethanol (twice). White solid. Yield: 2.23 g (80%). R_f (dichloromethane): 0.60. ^{1}H NMR (300 MHz, $CDCl_3$) δ: 1.20−1.45 (m, 28H), 1.60−1.70 (m, 4H), 1.70−1.82 (m, 4H), 4.00 (t, J = 6.6 Hz, 2H), 4.13 (t, J = 6.8 Hz, 4H), 4.31 (t, J = 6.6 Hz, 2H), 5.79 (dd, J = 10.4 Hz, J = 1.5 Hz, 2H), 6.10 (dd, J = 17.2, 10.4 Hz, 2H), 6.37 (d, J = 17.2 Hz, 2H), 6.98 (d, J = 8.8 Hz, 2H), 7.30 (d, J = 8.6 Hz, 2H), 7.58 (d, J = 8.8 Hz, 2H), 7.68 (d, J = 8.4 Hz, 2H), 8.12 (d, J = 8.6 Hz, 2H), 8.22 (d, J = 8.4 Hz, 2H). ^{13}C NMR (300 MHz, $CDCl_3$): 166.3, 166.0, 164.6, 159.9, 146.4, 131.2, 130.8, 130.1, 128.9, 128.5, 126.7, 121.8, 115.2, 83.9, 68.3, 65.3, 64.7, 52.5, 34.5, 29.5, 29.4, 29.3, 28.8, 28.7, 26.1, 26.0. IR (NaCl) ν_{max}/cm^{-1}: 1736, 1724, 1466, 1294, 1273, 1207, 831, 764. MS FAB+ *m*/*z*: 136, 176, 197, 349, 421, 782. Calcd. for $C_{48}H_{62}O_9$: C, 73.63; H, 7.98. Found: C, 73.67; H, 7.90.

(c) Synthesis of Compound ***f****. 4′-n-Decyloxy-4-biphenylcarboxylic Acid* ***11***. A mixture of methyl 4′-hydroxy-4-biphenylcarboxylate (3.50 g, 15.33 mmol), potassium hydroxide (0.99 g, 17.6 mmol), and potassium iodide (catalytic amount) in ethanol (25 mL) was stirred at room temperature for 1 h. Decyl bromide (3.39 g, 15.33 mmol) was added and the mixture was refluxed for 24 h. A solution of potassium hydroxide (2.58 g, 46.0 mmol) in water (30 mL) was added and the reaction mixture was refluxed for 3 h and then allowed to cool to room temperature. The precipitate was filtered off and suspended in a mixture of ethanol/water (1:1). Concentrated HCl was added until an acidic pH was attained and the resulting suspension was refluxed for 2 h. The reaction mixture was allowed to cool to room temperature and the precipitate was filtered off. The crude product was washed with water and recrystallized from ethanol. White solid. Yield: 4.23 g (78%). mp: 163 °C. R_f (1:1 hexane/ethyl acetate): 0.54. ^{1}H NMR (300 MHz, DMSO-d_6) δ: 0.80−0.90 (m, 3H), 1.20−1.50 (m, 14H), 1.65−1.80 (m, 2H), 4.00 (t, J = 6.4 Hz, 2H), 7.02 (d, J = 8.5 Hz, 2H), 7.66 (d, J = 8.5 Hz, 2H), 7.73 (d, J = 8.5 Hz, 2H), 7.96 (d, J = 8.5 Hz, 2H). IR (NaCl) ν_{max}/cm^{-1}: 3500−2500, 1685, 1290, 835, 770.

4′-n-Decyloxy-4-biphenylcarboxyl Chloride ***12***. Thionyl chloride (1.9 mL) was added to a mixture of 4′-decyloxy-4-biphenylcarboxylic acid (1.27 g, 3.57 mmol) and DMF (5 drops) under nitrogen. The mixture was refluxed for 3 h under nitrogen and the excess thionyl chloride was removed by distillation under reduced pressure. The resulting yellow solid was used without further purification. IR (NaCl) ν_{max}/cm^{-1}: 1739, 1597, 1463, 1379, 1263, 1187, 1027, 883, 827.

(R)-(1′-Methyl)heptyl 4-Benzyloxybenzoate ***13***. A solution of diethyl azodicarboxylate (7.63 g, 43.81 mmol) in dry dichloromethane (80 mL) was added dropwise to a solution of 4-benzyloxybenzoic acid (8.00 g, 35.05 mmol), (*S*)-(+)-2-octanol (5.48 g, 42.06 mmol) and triphenylphosphine (11.95 g, 45.57 mmol) in dry dichloromethane (240 mL) under nitrogen. The reaction mixture was stirred at room temperature for 24 h. After this time, water (a few drops) was added and the mixture stirred for an additional 1 h. The solvent was removed in vacuo and the resulting solid was stirred in a mixture of hexane/ethyl acetate (7:3) (200 mL) for 1 h. The white precipitate was filtered off and the solvent removed in vacuo. The crude product was purified by column chromatography (hexane/dichloromethane 3:1 to dichloromethane). Yellow oil. Yield: 5.13 g (43%). R_f (dichloromethane): 0.80. ^{1}H NMR (300 MHz, $CDCl_3$) δ: 0.80−0.95 (m, 3H), 1.20−1.50 (m, 11H), 1.55−1.70 (m, 1H), 1.70−1.82 (m, 1H), 5.11 (s, 1H), 5.05−5.20 (m, 1H), 6.98 (d, J = 8.1 Hz, 2H), 7.30−7.45 (m, 5H), 8.01 (d, J = 8.1 Hz, 2H). IR (NaCl) ν_{max}/cm^{-1}: 1708, 1605, 1508, 1277, 1250, 1167, 1102, 846, 770.

(R)-1′-Methylheptyl 4-Hydroxybenzoate ***14***. Palladium hydroxide (0.50 g, 10% w/w) was added in small portions to a refluxing solution of (*R*)-1′-methylheptyl 4-benzyloxybenzoate (5.01 g, 14.72 mmol) in ethanol (115 mL) and cyclohexene (58 mL). The reaction mixture was refluxed for 3 h and filtered through Celite. The solvent was removed in vacuo and the

crude product purified by column chromatography (dichloromethane). Yellow oil. Yield: 3.57 g (97%). R_f (dichloromethane): 0.48. ^{1}H NMR (300 MHz, $CDCl_3$) δ: 0.80−0.90 (m, 3H), 1.20−1.42 (m, 11H), 1.50−1.62 (m, 1H), 1.62−1.75 (m, 1H), 5.05−5.15 (m, 1H), 5.57 (s, 1H), 6.83 (d, J = 8.8 Hz, 2H), 7.94 (d, J = 8.8 Hz, 2H). IR (film) ν_{max}/cm^{-1}: 3396, 1677, 1605, 1512, 1281, 1271, 852, 775.

*(R)-1″-Methylheptyl 4-(4′-n-Decyloxybiphenyloxy)benzoate (**f**).* A mixture of 4-*n*-decyloxybenzoic acid (1.24 g, 4.45 mmol), thionyl chloride (2.10 mL), and DMF (catalytic amount) was refluxed for 3 h under nitrogen. The excess thionyl chloride was removed under reduced pressure. 4-Decyloxybenzoyl chloride was obtained as a yellow solid (1.27 g, 3.57 mmol), dissolved in dry dichloromethane (15 mL), and added slowly to a solution of (*R*)-1′-methylheptyl 4-hydroxybenzoate (0.88 g, 3.50 mmol) and triethylamine (0.79 mL, 0.46 g, 5.35 mmol) in dry dichloromethane (50 mL) under nitrogen. The mixture was stirred at room temperature for 24 h and then filtered. The solvent was removed in vacuo and the crude product was purified by column chromatography (hexane/dichloromethane 1:1) and recrystallization first from ethanol and then from acetonitrile. White solid. Yield: 1.54 g (75%). R_f (dichloromethane): 0.82. ^{1}H NMR (300 MHz, $CDCl_3$) δ: 0.85−0.95 (m, 6H), 1.20−1.90 (m, 29H), 4.02 (t, J = 6.6 Hz, 2H), 5.10−5.20 (m, 1H), 7.00 (d, J = 8.8 Hz, 2H), 7.31 (d, J = 9.0 Hz, 2H), 7.60 (d, J = 8.8 Hz, 2H), 7.70 (d, J = 8.8 Hz, 2H), 8.13 (d, J = 9.0 Hz, 2H), 8.24 (d, J = 8.8 Hz, 2H). ^{13}C NMR ($CDCl_3$) δ: 165.5, 164.6, 159.6, 154.5, 146.2, 131.8, 131.2, 131.1, 130.8, 128.4, 128.3, 127.0, 126.6, 121.8, 121.6, 115.1, 114.9, 72.0, 71.8, 68.2, 36.1, 31.9, 31.7, 29.6, 29.3, 29.2, 26.0, 25.4, 22.6, 20.1, 14.1, 14.0. IR (NaCl) ν_{max}/cm^{-1}: 1730, 1715, 1465, 1270, 765, 690. MS FAB+ *m*/*z*: 55, 69, 141, 169, 197, 337, 586. Calcd. for $C_{38}H_{50}O_5$: C, 77.78; H, 8.59. Found: C, 77.74; H, 8.61. $[\alpha]_D^{22}$ −58.5 (c = 1.01, $CHCl_3$).

In Situ Photopolymerization. The photopolymerizable samples were prepared by dissolving the appropriate proportions of **f** and the direactive monomers, 0.5% (weight) of the photoinitiator IRGACURE 369 (CIBA Geigy) and 200 ppm of 2,6-di-*tert*-butyl-4-methylphenol (thermal inhibitor) in freshly distilled dichloromethane. The solvent was evaporated at room temperature and the residual solvent was removed by heating the sample at 30 °C under vacuum overnight.

In situ photopolymerization was studied by DSC using a Perkin-Elmer DSC-7 suitably modified for the study of photopolymerization processes: 2−6 mg of photopolymerizable sample was placed in an open aluminum DSC pan. Experiments were carried out under a nitrogen atmosphere to avoid oxygen inhibition. A UV lamp (Philips PL-S 9W/10), at a distance of 13 cm from the sample and reference holders, was used to irradiate the samples. The sample was heated to a temperature slightly above the isotropization point and then to the selected polymerization temperature, at which the sample was maintained for 5 min before irradiation under isothermal conditions. Irradiation was maintained for 15 min and the photopolymerization was detected as an exotherm in the DSC trace. The degree of conversion was calculated from the enthalpy content of this polymerization peak, taking 78 kJ/mol as the polymerization enthalpy of 1 mol of acrylate group.[18]

Samples were also photopolymerized in commercial cells (Linkam, UK) and coated with polyimides, which have a cell gap of d = 7.5 μm and promote parallel alignment to produce oriented polymeric films for dielectric and optical measurements. The samples were introduced by capillary action at a temperature of 10 °C above the clearing point. To obtain a uniform alignment, the cells were slowly cooled (0.1 °C/min) from the isotropic phase to the phase in which the photopolymerization was desired. In all cases a defect-free planar monodomain was observed by microscopy. The mixtures were then irradiated with a UV-A Philips PL-S 9W/10 (λ = 365 nm) lamp placed 5 cm from the cell and irradiation was maintained for 15 min.

Experimental Details of the Dielectric and Optical Measurements. The dielectric permittivities of the antiferroelectric pure compound **f** and the gels were obtained with an impedance analyzer (HP4192A). For the pure compound we used two different cells: the aforementioned cells, purchased from Linkam, and another that consisted of two metallic electrodes separated by 50-μm silica spacers to allow a better dielectric characterization.

To analyze the switching process, the glass cells were placed between crossed polarizers so that the sample appeared dark (in the SmC^*_A) in the field-off state (optical axis coincides with the layer normal) and became bright if the optical axis (molecular director) was tilted by θ or $-\theta$ due to the application of the electric field. We recorded the transmittance versus the applied electric field (triangular wave, 0.5 Hz).

In addition, we measured the current through the cell during the switching process (triangular wave, 50 Hz) and from these data we calculated the spontaneous polarization.

Techniques. Optical absorption measurements were taken using an ATI Unicam UV4 spectrophotometer. Infrared spectra for all the complexes were obtained using a Perkin-Elmer 1600 (FTIR) spectrophotometer in the 400−4000-cm^{-1} spectral range. ^{1}H and ^{13}C NMR spectra were recorded on Varian Unity 300 MHz and Bruker ARX-300 MHz spectrometers and samples were in solution. Microanalysis was performed with a Perkin-Elmer 2400 microanalyzer. Mass spectrometry studies (EI and FAB+) were performed with a VG AutoSpec EBE. Polarimetry measurements were performed using a Perkin-Elmer 241-AC polarimeter.

Mesomorphic properties were studied by optical microscopy using an Olympus BH2 microscope with crossed polarizers. The microscope was connected to a Linkam THMS 600 hot stage. Transition temperatures were determined by differential scanning calorimetry (DSC) using either a TA2910 differential calorimeter or Perkin-Elmer DSC-7. Each apparatus was calibrated with indium (156.6 °C, 28.44 J/g) and tin (232.1 °C, 60.5 J/g) using a scanning rate of 10 °C/min in most cases. X-ray diffraction patterns were obtained with an evacuated Pinhole Camera (Anton-Paar) operating with a point-focused Ni-filtered Cu Kα beam. The samples were held in Lindemann glass capillaries (1-mm diameter) and heated, when necessary, with a variable-temperature attachment. The diffraction patterns were collected on flat photographic film.

Acknowledgment. This work was supported by the Spanish Government through project CICYT MAT97-0986-C01-C02 and MAT99-1009-C02 and by the Universidad del País Vasco through project UPV060.310-G16/98.M. C. Artal thanks the Spanish Comisión Interministerial de Ciencia y Tecnología (CICYT) for her grant.

CM001254M

(18) Tryson, G. R.; Shultz, A. R. *J. Polym. Sci., Polym. Phys. Ed.* **1979**, *17*, 2059.